KAPL-P-000005
(K95040)

PREDICTION OF PURE WATER STRESS CORROSION CRACKING (PWSCC) IN NICKEL BASE ALLOYS USING CRACK GROWTH RATE MODELS

C. D. Thompson, H. T. Krasodomski, N. Lewis, G. L. Makar

February 1995

NOTICE

KAPL ATOMIC POWER LABORATORY SCHENECTADY, NEW YORK 12301

Operated for the U. S. Department of Energy
by KAPL, Inc. a Lockheed Martin company

DISCLAIMER

DISCLAIMER

Portions of this document may be illegible in electronic image products. Images are produced from the best available original document.

Prediction of PWSCC in Nickel Base Alloys Using Crack Growth Rate Models

Charles D. Thompson
Henry T. Krasodomski
Nathan Lewis
Gregory L. Makar
Knolls Atomic Power Laboratory
P. O. Box 1072
Schenectady, NY 12301

February 22, 1995

Abstract

The Ford/Andresen slip dissolution SCC model, originally developed for stainless steel components in BWR environments, has been applied to Alloy 600 and Alloy X-750 tested in deaerated pure water chemistry. A method is described whereby the crack growth rates measured in compact tension specimens can be used to estimate crack growth in a component. Good agreement was found between model prediction and measured SCC in X-750 threaded fasteners over a wide range of temperatures, stresses, and material condition. Most data support the basic assumption of this model that cracks initiate early in life.

The evidence supporting a particular SCC mechanism is mixed. Electrochemical repassivation data and estimates of oxide fracture strain indicate that the slip dissolution model can account for the observed crack growth rates, provided primary rather than secondary creep rates are used. However, approximately 100 cross-sectional TEM foils of SCC cracks including crack tips reveal no evidence of enhanced plasticity or unique dislocation patterns at the crack tip or along the crack to support a classic slip dissolution mechanism. No voids, hydrides, or microcracks are found in the vicinity of the crack tips creating doubt about classic hydrogen related mechanisms. The bulk oxide films exhibit a surface oxide which is often different than the oxides found within a crack. Although bulk chromium concentration affects the rate of SCC, analytical data indicates the mechanism does not result from chromium depletion at the grain boundaries. The overall findings support a corrosion/dissolution mechanism but not one necessarily related to slip at the crack tip.

Key terms: Alloy 600, Alloy X-750, predictive models, mechanism, stress corrosion cracking

Introduction

This paper describes the application of the slip-dissolution model to the pure water stress corrosion cracking (PWSCC) of nickel base alloys. This model was first developed by D. Vermilyea[1] and later applied to stress corrosion cracking of stainless steel in boiling water reactor conditions by P.Ford and P. Andresen[2,3]. The paper covers four aspects of SCC modeling: demonstration that the model fits existing Alloy 600 crack growth data, demonstration that the model gives reasonable estimates for A600 crack growth rates based

solely on fundamental inputs, application of the model to predict component SCC, and mechanistic considerations.

The conceptual basis for the slip dissolution model assumes a step-wise process of crack advance that can be summarized as follows:

- Oxide film rupture at the crack tip due to time dependent strain (creep).
- Bare metal (anodic) dissolution at the crack tip.
- Repassivation at the crack tip due to reformation of the protective oxide.
- Continued deformation at the crack tip resulting in a new oxide rupture event that repeats the sequence.

Creep strain is the primary variable proposed to control the periodicity of the film rupture events. The rate of anodic dissolution and repassivation is determined by the alloy, the nature of its protective oxide, and the environment at the crack tip.

Mathematically, the rate of crack advance can be derived from Faraday's law as the depth "a" of metal that corrodes electrochemically within an increment of time:

$$da = \frac{M}{zpF} dQ_f = \frac{M}{zpF} idt \qquad (1)$$

where: da = depth of corrosion (cm)
M = molecular weight (g/mole)
p = density of metal (g/cm^3)
z = charge on the dissolving metal (equivalents/mole)
F = Faraday constant (96,500 coulombs/mole)
Q_f = charge density per film rupture event (coulombs/cm^2)
i = current density at the crack tip (amperes/cm^2)
t = time (seconds)

The repassivation current typically follows a power law:

$$i = i_o(\frac{t}{t_o})^{-n} \qquad for\ t_o < t < t_f \qquad (2)$$

where: i_o = bare metal current density (amps/cm^2)
t_f = time between rupture events
t_o = time at beginning of repassivation
n = repassivation rate parameter

The incremental growth for each rupture event (i.e., average crack growth rate) is:

$$V_{CT} = \frac{M}{zpF} \int_{t_o}^{t_f} i_o \left(\frac{t_o}{t_f}\right)^{-n} dt = \frac{M}{zpF} \frac{Q_f}{t_f} = \frac{M}{zpF} \frac{Q_f}{\epsilon_F} \dot{\epsilon}_{CT} \qquad (3)$$

where: ϵ_f = oxide fracture strain
$\dot{\epsilon}_{CT}$ = crack tip strain rate

Andresen also developed an empirical relationship which showed that $\dot{\epsilon}_{CT}$ is proportional to the stress intensity factor[2]. The average crack growth rate can be expressed generally as a function of n, ϵ_f, i_o, and stress intensity factor K_I:

$$V_{CT} = A\ \dot{\epsilon}_{CT}^{n} = A\ K_I^{4n} \qquad (4)$$

where A and n are parameters which are specific functions of the crack tip material and environment combinations.

Crack Growth Rates

To assess the applicability of the slip dissolution model to PWSCC of nickel alloys, a model was evaluated against an Alloy 600 primary water CGR database. Figure 1 provides a compilation of Alloy 600 CGR data from several sources[4,5,6,7], including KAPL generated data. This data is edited to include only actively loaded specimens to avoid the issue of stress relaxation in constant displacement specimens. Also shown is the model prediction for CGR vs. K_I using repassivation ratio (n) with values of 0.5 and 0.7. The functionality expressed by the Andresen model is in reasonable agreement with the observed trends.

On the basis of this fit of the data from the slip dissolution model, it was decided to examine some of the fundamental input parameters of the model as further evidence that the model is viable for PWSCC application of nickel base alloys.

Model Fundamental Parameters

The purpose of this section is to examine the slip dissolution model prediction of Alloy 600 crack growth rates based on the fundamental inputs. The four fundamental inputs (measured parameters) to the slip dissolution model are maximum bare metal dissolution current density (i_o), repassivation rate (n), creep rate (as a function of applied load), and oxide fracture strain.

Figure 2 shows a plot of log current vs. time for the repassivation of Alloy 600 wire at 288°C (550°F) in boric acid/sodium hydroxide with pH_{288} approximately 7.2. These data were obtained by stepping the applied potential to -0.711 V_{SHE} after 15 minutes at -1.5V_{SHE}. The plot indicates a lower bound bare metal current density of 3.5 mA/cm^2 and a repassivation parameter, "n", of 0.7. Similar results have been obtained using the drop weight method at the same potential, indicating that the Alloy 600 oxide found at the test condition is in fact reduced at the test conditions. This repassivation current is equivalent to those reported by Soji[8] at 288°C in 0.01M Na_2MoO_4, but the repassivation time is somewhat faster.

Crack growth rate data for Alloy 600 at 288°C (550°F) is not available. However, based on the data of Figure 1, a nominal value of 0.3 mils/day at 338°C (640°F) and at a K_1 of 25 ksi$\sqrt{in}$ is a reasonable baseline value to extrapolate to lower temperatures. Apparent activation energies for PWSCC of A600 range from 15 to 54 Kcal/mol depending on stress intensity factor and degree of cold work[9,10]. Extrapolation of 0.3 mils/day at 338°C to 288°C (550°F) with this range of activation energies yields crack growth rates of 0.01 mils/day (Q = 54) to 0.1 mils/day (Q = 15).

Figure 3 presents the predicted crack growth rate of A600 from the slip dissolution model as a function of the periodicity of the film rupture. A periodic rupture time (t_f) of about 550 seconds would be required for a crack growth rate of 0.1 mils/day, whereas a t_f of 26,000 results in a calculated rate of 0.01 mils/day.

An oxide fracture strain of 0.003, approximately equal to the base metal yield strain, represents an order of magnitude estimate for mixed spinel oxides at 80°F, and it is assumed that this value is independent of temperature up to 550°F. For a crack tip strain rate $\dot{\epsilon}_{CT} = \epsilon_f/t_f$, and ϵ_f = 0.003, the resulting creep strain rate would be calculated to be between 4.2 x 10^{-6} to 1.1 x 10^{-7} (sec^{-1}). These strain rates are 2-3 orders of magnitude higher than the steady state (secondary) strain rates predicted by Garud for Alloy 600[11]. However, with the t_f being between 9.2 minutes and 7.2 hours, primary creep appears to be dominant with predicted strain rates between 10^{-6} and 10^{-8} (sec^{-1}), which is in agreement with the required crack tip strain rate to maintain the required crack growth rates predicted by an anodic dissolution mechanism.

The general conclusion from this analysis is that the slip dissolution model yields reasonable estimates of Alloy 600 crack growth rates based on fundamental input parameters provided primary creep rates are considered dominant rather than secondary creep rates.

Prediction of Component SCC Endurance

KAPL has developed an engineering method to relate actual component SCC endurance to laboratory crack growth rates. The needed input data consists of measured crack growth rates as a function of stress intensity factor for the material of interest at the temperature of interest. It is assumed that crack growth initiates at time zero in a very small initial flaw. We have generally assumed an initial flaw size of 0.0001" (0.00025 cm) and have found that the calculated crack lengths are fairly insensitive to the initial flaw size assumptions. The general process consists of the following steps:

- Assume initial small flaw size.
- Calculate K_I for initial flaw and given load.
- Calculate corresponding crack growth rate.
- Calculate amount of crack growth for an incremental period of time at the K_I.
- Advance the crack by the given amount.
- Recalculate K_I and repeat the process.

SCC data is necessary on both laboratory compact tension specimens and full size components for matching material/environment conditions. Such data has been obtained by KAPL for X-750 condition AH. Figure (4) presents KAPL crack growth rate data on Condition AH X-750 obtained from 0.4T CT specimens under constant load at 315-360°C (600-680°F). Correlating predictions are also plotted against the data. A K_I^{2a} correlation was found to be better than K_I^{4a} for this material/environment combination.

The laboratory crack growth rates and correlating model has been used to assess the SCC of threaded fasteners. This model prediction is shown in Figure (5) and is superimposed on the measured crack depth data for specimens tested at 338°C (640°F). Another prediction and matching fastener data for 282°C (540°F) is shown in Figure (6). Crack lengths in the fasteners were determined by destructive metallographic examination. Figure (7) compares the predicted crack lengths to the observed crack length for 88 specimens over a wide range of test conditions with applied stresses from 28 to 103 ksi and test temperatures from 282 to 360°C (540 to 680°F). Good predictive agreement is obtained over a wide range of measured crack lengths (from about 3 to 123 mils). The general agreement is within 2X and it is concluded that the CGR modelling process can provide reasonable predictions of SCC in plant components provided quality CGR data is available.

Physical Evidence

Figure 8 shows an AEM cross-sectional image of an Alloy 600 specimen tested at 338°C (640°F). The foil preparation process is described in Reference (12). The significant observation is lack of indication of any deformation associated with the crack process. Figure 9 shows an SCC crack tip on a grain boundary without carbides with no evidence of voids or grain boundary sliding often associated with creep. To date, more than 100 AEM foils from 50

separate A600 specimens have been analyzed. We have found no voids, hydrides, or microcracks ahead of the crack tip, commonly cited as indications of a hydrogen related SCC mechanism. The lack of unique deformation associated with the crack tip casts doubt on slip or creep as a participant in the SCC mechanism.

The bulk oxide films exhibit a surface oxide which is often different than the oxides found within a crack. Surface oxides are Cr and Ni rich near the metal surface and contain NiO and spinels in the outer layers. In a number of instances, NiO is found within the crack adjacent to the metal which is not observed at the bulk specimen oxide/metal interface (Figure 10).

The presence of oxides at the crack tip is an indication that oxidation is taking place as a result of exposure to the environment. The differing oxides inside the crack as compared to the outside surface suggests a difference in the environment and/or material (grain boundary) at the tip. The changes in the oxide composition inside the crack suggests non-uniformity in solubility and probably repassivation kinetics. These observations taken as a whole suggest an oxide fracture/dissolution mechanism for crack propagation, but not one associated with slip at the crack tip.

Conclusions

- The slip-dissolution model provides an adequate engineering fit to the measured crack growth rates for Alloy 600 in pure/primary water.
- Based solely on fundamental inputs, the slip dissolution model gives reasonable estimates for A600 crack growth rates, provided primary creep rate values are inputed.
- An engineering model (independent of mechanisms) that uses laboratory crack growth rate data provides a sound basis to predict the SCC endurance of actual components.
- Issues pertaining to the application of the slip dissolution model to PWSCC of nickel alloys include lack of evidence of plastic deformation uniquely associated with the crack tip, understanding oxide changes as a function of grain boundary microstructure and chemistry, and the rates of creep deformation.

Acknowledgements

This work was performed at Knolls Atomic Power Laboratory, operated for the U. S. Department of Energy by KAPL, Inc., Martin Marietta Corporation, under contract DE-AC12-76SN00052. The repassivation studies were performed by subcontract at General Electric Corporate Research & Development.

References

1. DA Vermileya and DB Diegle, "Concerning Strain Enhanced Corrosion Mechanisms of SCC", Corrosion Vol. 32, No. 1, 1976.

2. FP Ford, DF Taylor, PL Andresen, "Corrosion-Assisted Cracking of Stainless and Low-Alloy Steels in LWR Environments", EPRI NP-5064M, 1987.

3. PL Andresen, "Fracture Mechanics Data and Modeling of Environmental Cracking of Nickel Base Alloys in High Temperature Water", Corrosion, Vol. 47, No. 12, 1991.

4. TB Cassagne and A. Gelpi, "Crack Growth Rate Measurements on Alloy 600 Steam Generator Tubes in Primary and Hydrogenated AVT Water", Proceedings - 6th International Symposium on Environmental Degradation of Materials in Nuclear Power Systems - Water Reactors, 1993.

5. RG Lott, RJ Jacko, RE Gold, "Primary Water Stress Corrosion Crack Growth Rates in Alloy 600 Steam Generator Tubing", Proceedings - 5th International Symposium on Environmental Degradation of Materials in Nuclear Power Systems - Water Reactors, 1991.

6. W Bamford, J Foster, "Alloy 600 Penetration Crack Growth Program" Primary Water Stress Corrosion Cracking of Alloy 600 in PWR's, EPRI, Tampa, Florida, November 15-17, 1994.

7. RB Rebak, AR McIlree, and Z. Szklarska-Smialowska, "Effects of pH and Stress Intensity on Crack Growth Rate in Alloy 600 in Lithiated + Borated Water at High Temperatures", Proceedings - 5th International Symposium on Environmental Degradation of Materials in Nuclear Power Systems - Water Reactors, 1991.

8. T Shoji, "Mechanics and Mechanisms of Stress Corrosion Cracking of Alloy 600 in High Temperature Waters", EPRI Workshop: Specialists Meeting on Environmental Degradation of Alloy 600, Warrenton, Virginia, April 1993.

9. Y Shen and PG Shewmon, "IGSCC Crack Growth of Alloy 600 and X-750 in Steam", Corrosion-NACE, Vol. 47, No. 9, p 712, 1991.

10. RO Speidel and R Magdowski, "Stress Corrosion Cracking of Nickel Base Alloys", Institute of Metallurgy, Swiss Federal Institute of Technology, 6th International Symposium on Environmental Degradation of Materials in Power Systems - Water Reactors, 1993.

11. YS Garud, "Development of a Model for Predicting Intergranular Stress Corrosion Cracking of Alloy 600 Tubes in PWR Primary Water", EPRI NP-3791, 1985.

12. N Lewis, B Bussert, M Bunch, "Cross Sectional AEM Analysis of SCC Cracks", EPRI Steam Generator IGA/SCC Workshop, December 8-10, San Antonio, Texas, 1992.

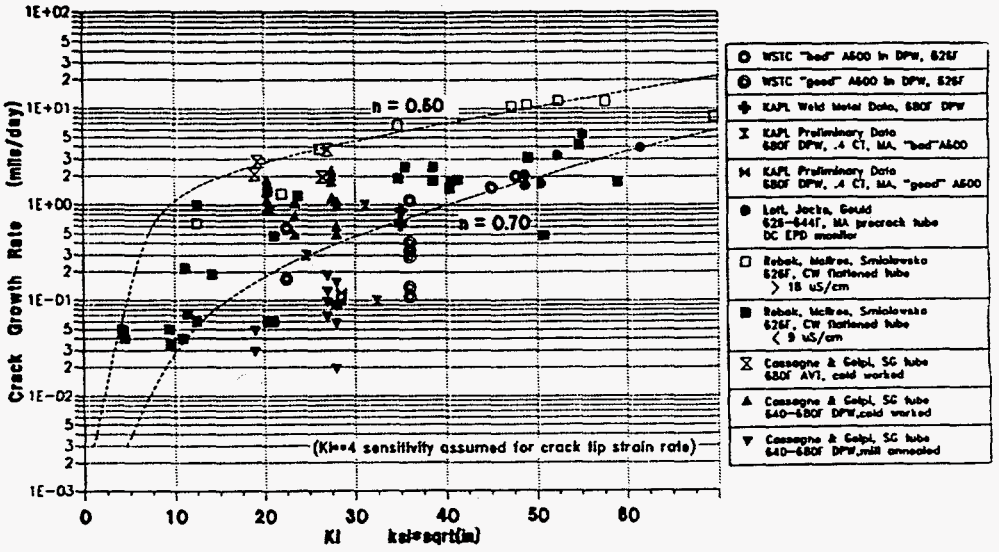

Figure 1. Compilation of Alloy 600 crack growth rate data in high temperature deaerated pure water and Ford/Andresen model correlation for crack growth rate vs. K_I for 'n' values of 0.5 and 0.7.

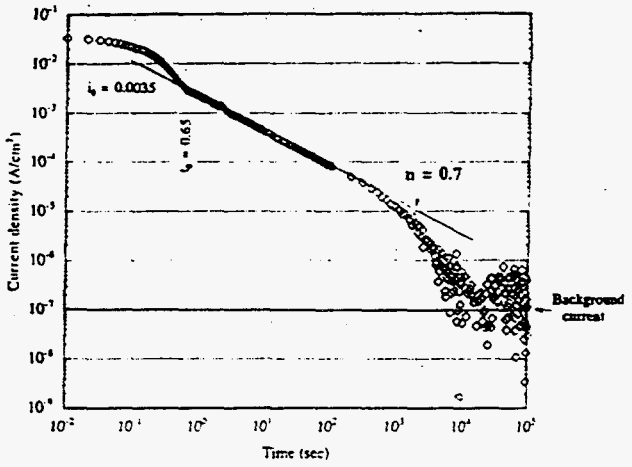

Figure 2. KAPL repassivation data on Alloy 600, potential pulse from -1500mV$_{SHE}$ to -711mV$_{SHE}$ at 288°C, deaerated 0.1M boric acid titrated with NaOH to a cell resistance of 105 ohms and pH=7.6 at 25°C.

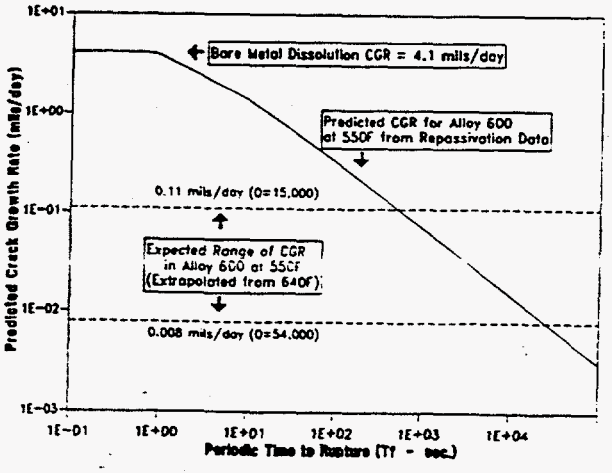

Figure 3. Predicted crack growth rate from repassivation data as a function of the periodic oxide rupture time.

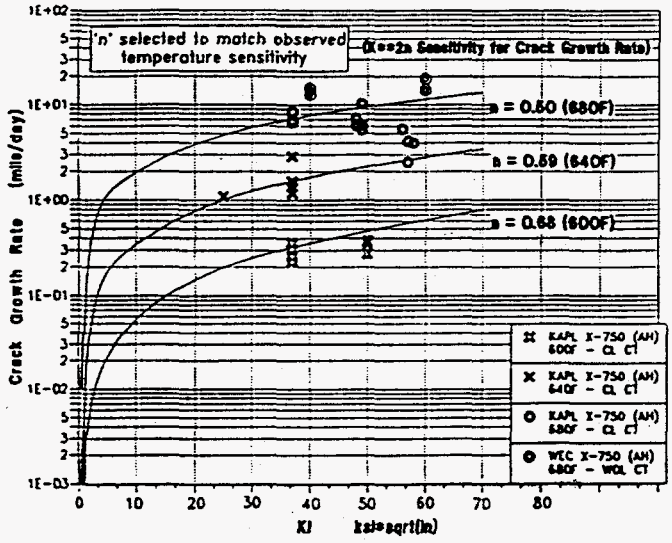

Figure 4. Crack growth rate data for X-750, Condition AH in high temperature deaerated pure water, constant load 0.4T CT specimens.

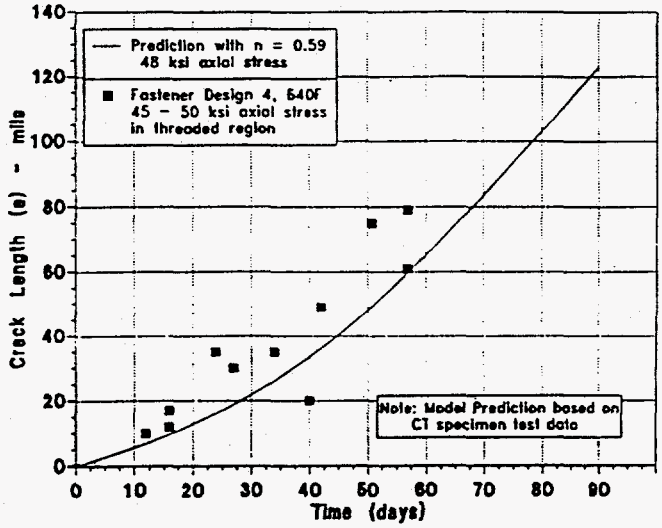

Figure 5. Model prediction of crack depth based on CT specimen data and corresponding observations for X-750, Condition AH threaded fasteners tested in DPW at 640°F.

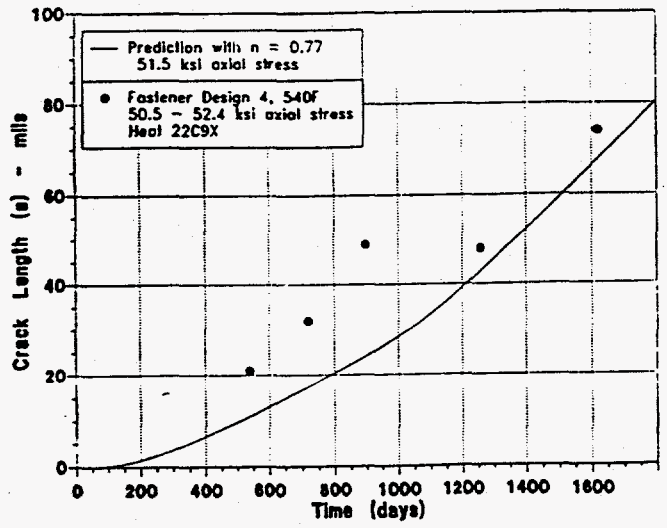

Figure 6. Model prediction of crack depth and corresponding for X-750, Condition AH threaded fasteners tested in DPW at 540°F.

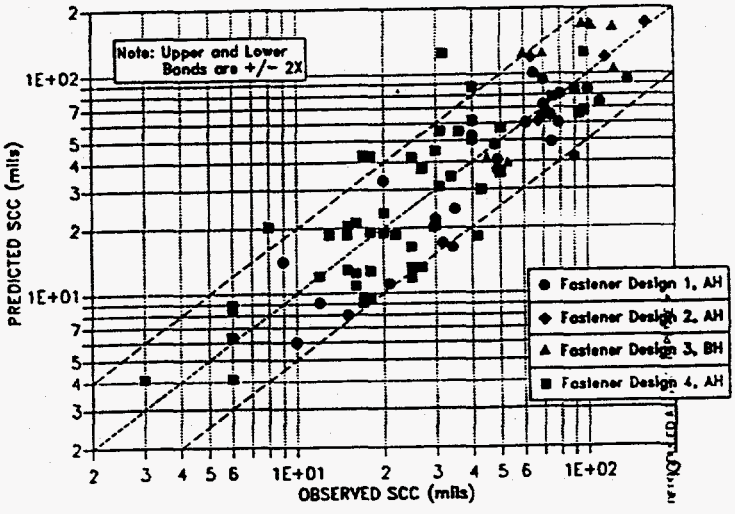

Figure 7. Predicted crack length based on CT specimen data versus observed crack length for wide range of fastener geometries, applied stress, and temperature.

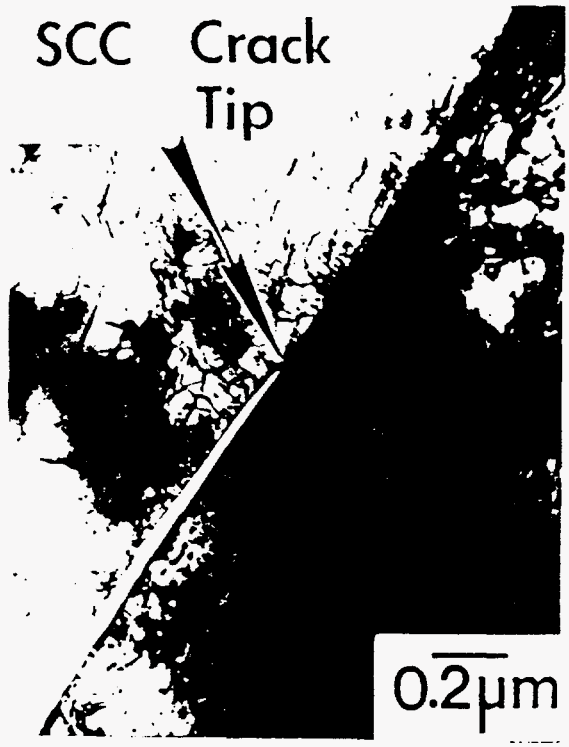

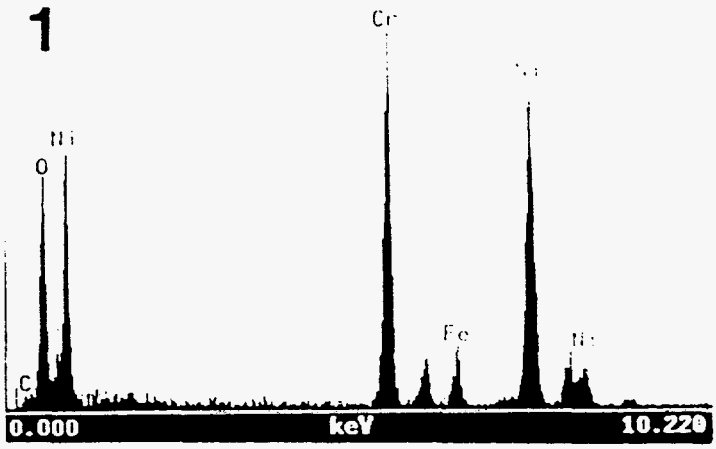

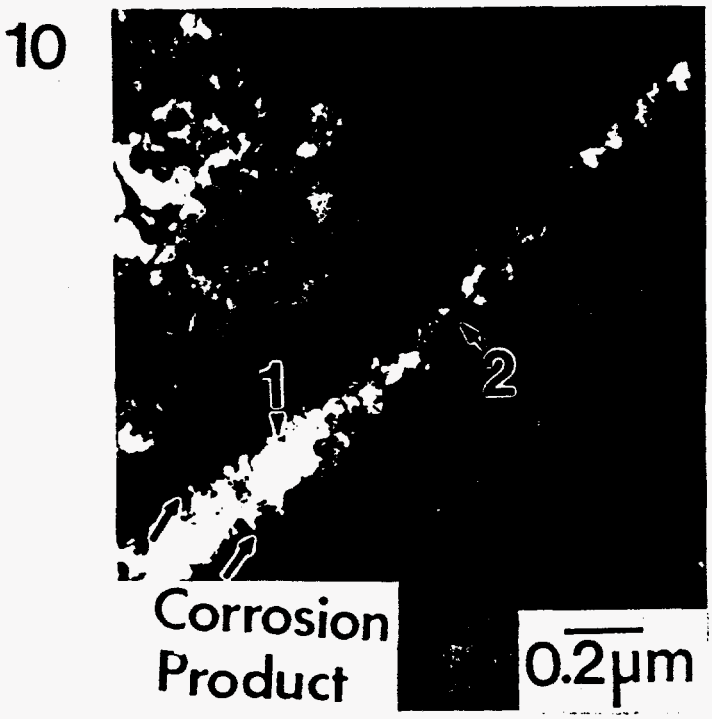

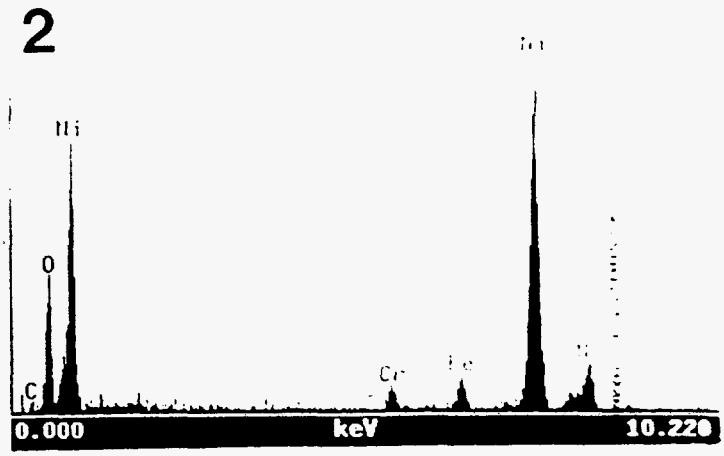

FIGURE 8. AEM CROSS-SECTIONAL IMAGE SHOWING SCC CRACK PROPAGATING AROUND COMPLEX GRAIN BOUNDARY CONTAINING Cr_7C_3 CARBIDES. NOTE AS CRACK CHANGES DIRECTION DISLOCATION STRUCTURE REMAINS THE SAME. FIGURE 9. SCC CRACK TIP. NO CARBIDES, VOIDS OR MICROCRACKS OBSERVED AHEAD OF CRACK. FIGURE 10. CORROSION PRODUCT IN SCC CRACK CONTAINING BOTH CR AND NI RICH OXIDE AND NIO.

STRESS CORROSION CRACKING INITIATION

- 502 Double U-bend & 112 C-ring specimens
- EN62, EN82 weld metal
- Tested at 600°F, 640°F, 680°F (315, 338, 360°C) for up to 249 weeks
- Four strain levels;
  10% and 16% for U-bends
  .45% and 4% for C-rings

SCC Initiation - Results

Thermal treatment of weld metal (1125°F (607°C) for 7 hours)

- Beneficial in reducing SCC
- Statistically - 95% confidence of a significant difference
- 56% of non-thermal treated specimens failed
- 21% of thermally treated specimens failed

FIGURE 11

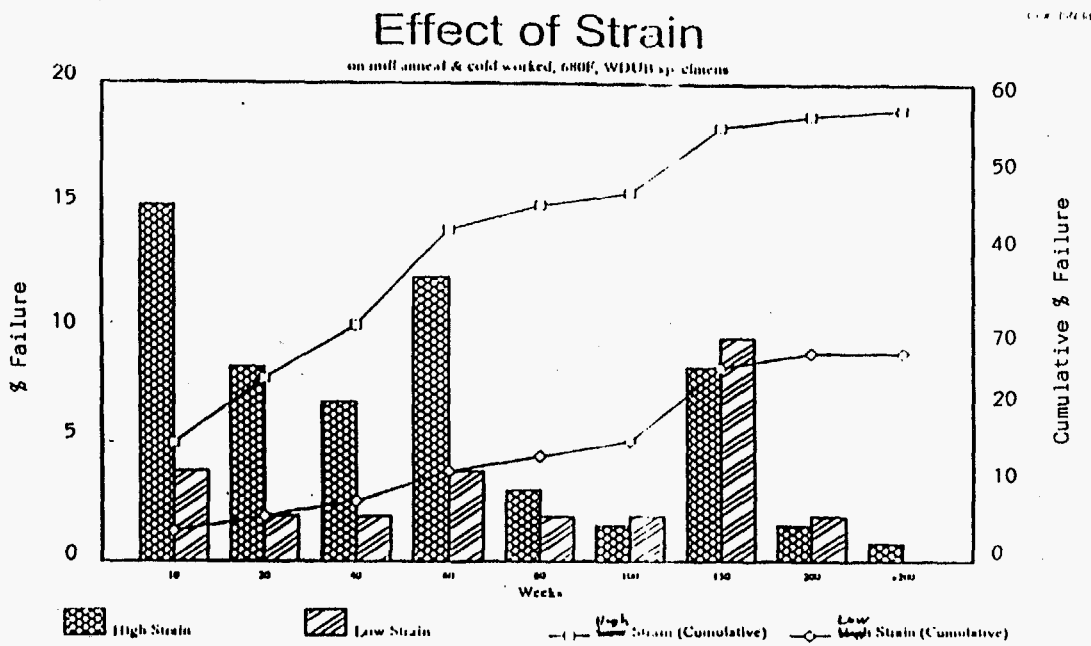
Effect of Strain
% Failure
Cumulative % Failure
Weeks
High Strain
Low Strain

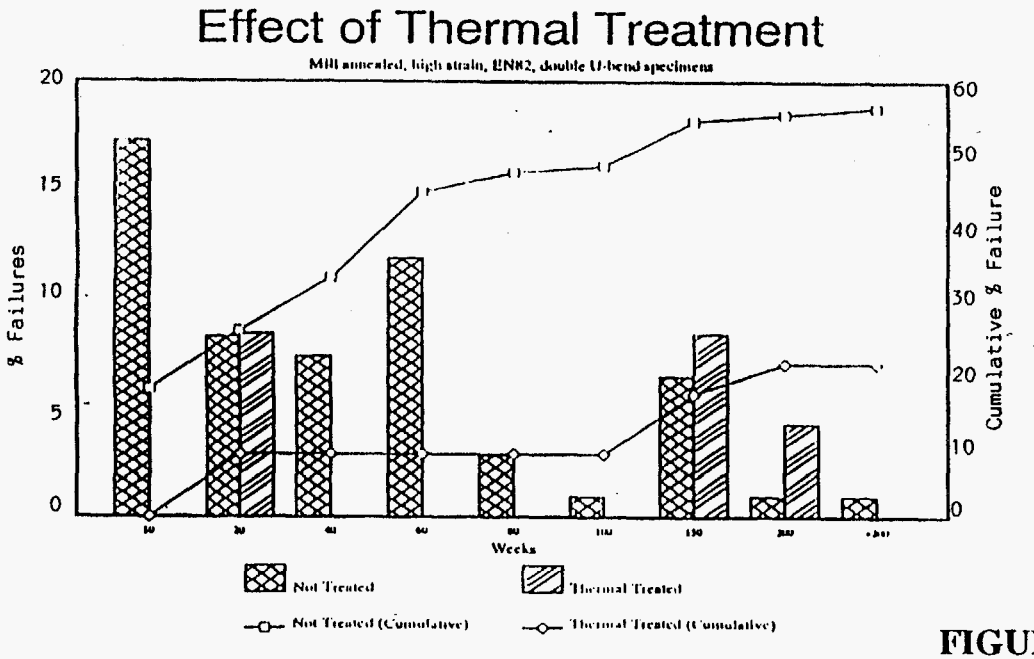
Effect of Thermal Treatment
Mill annealed, high strain, EN82, double U-bend specimens
% Failures
Cumulative % Failure
Weeks
Not Treated
Thermal Treated

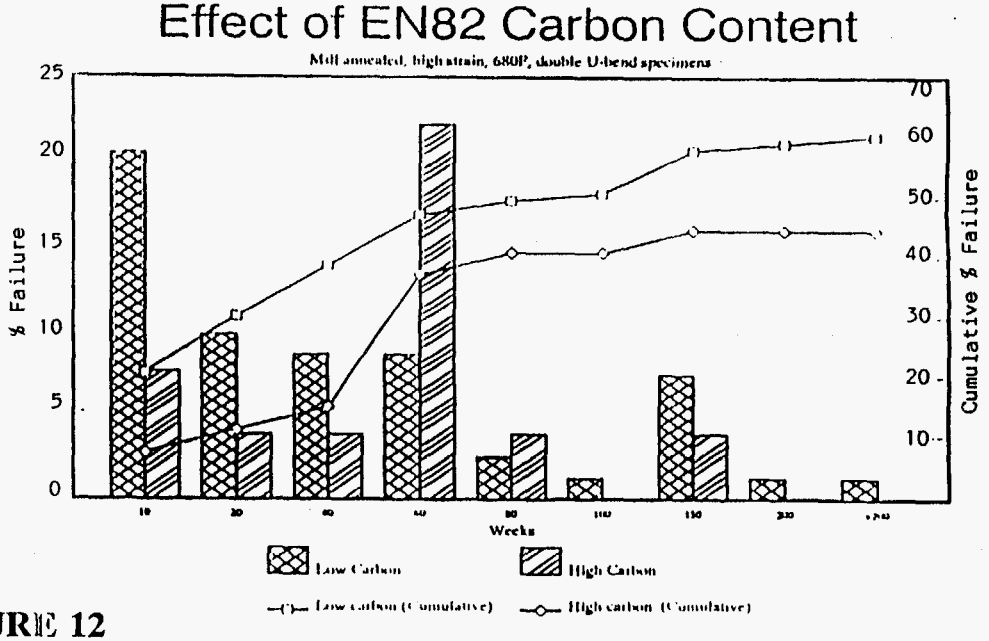
Effect of EN82 Carbon Content
Mill annealed, high strain, 680F, double U-bend specimens
% Failure
Cumulative % Failure
Weeks
Low Carbon
High Carbon

FIGURE 12

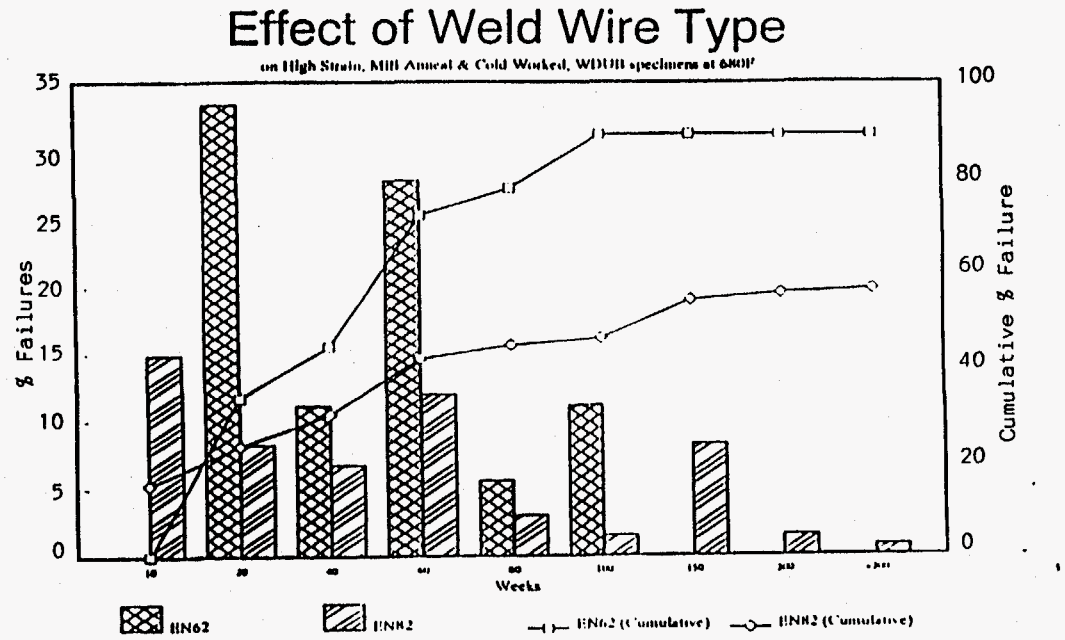
Effect of Weld Wire Type
on High Strain, Mill Anneal & Cold Worked, WDUB specimens at 680F
% Failures
Cumulative % Failure
Weeks
35
30
25
20
15
10
5
0
100
80
60
40
20
0
IN62
IN82
IN62 (Cumulative)
IN82 (Cumulative)

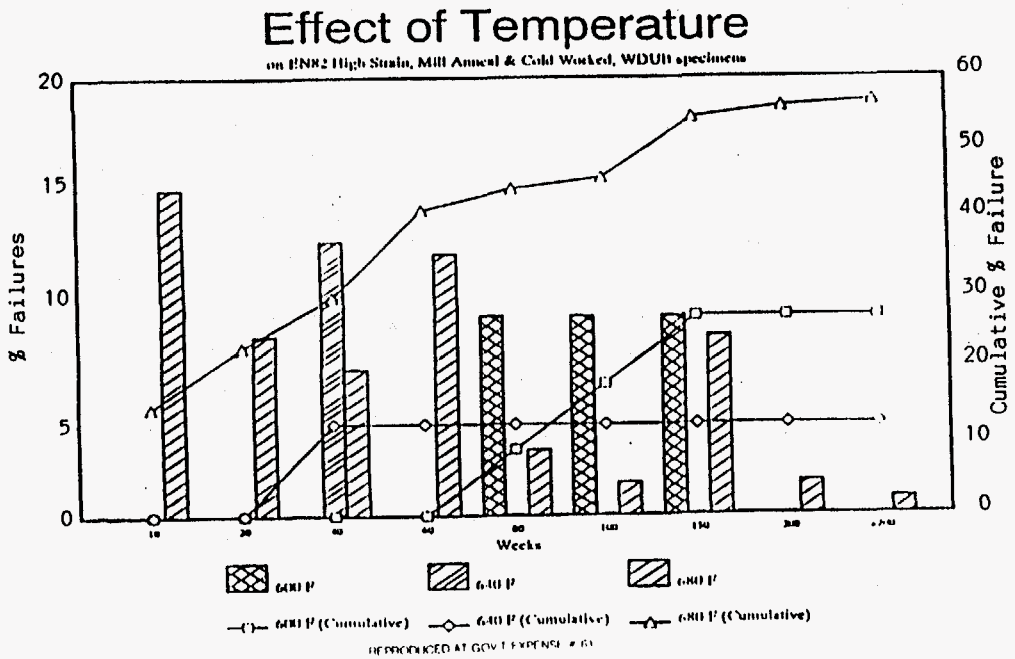
Effect of Temperature
on IN82 High Strain, Mill Anneal & Cold Worked, WDUB specimens
% Failures
Cumulative % Failure
Weeks
20
15
10
5
0
60
50
40
30
20
10
0
600 F
640 F
680 F
600 F (Cumulative)
640 F (Cumulative)
680 F (Cumulative)

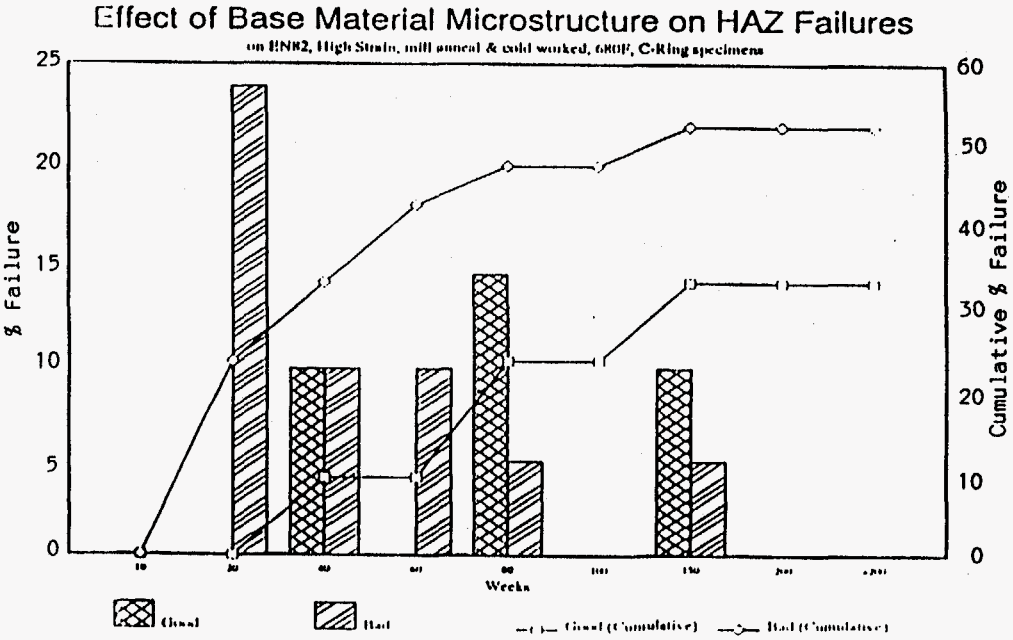
Effect of Base Material Microstructure on HAZ Failures
on IN82, High Strain, mill anneal & cold worked, 680F, C-Ring specimens
% Failure
Cumulative % Failure
Weeks
25
20
15
10
5
0
60
50
40
30
20
10
0
Good
Bad
Good (Cumulative)
Bad (Cumulative)

FIGURE 13

STRESS CORROSION CRACK GROWTH RATE TESTING

- 3 - .4T precracked compact tension specimens
- EN82 weld metal
- Constant load - stress intensity of 35 ksi$\sqrt{in}$ (38 MPa$\sqrt{m}$)
- 680°F (360°C) primary water for 108 days

Results/Conclusions

- Specimens showed a range of growth rates of 0.62 to 1.08 mils/day (1.8×10^{-10} to 3.2×10^{-10} m/s)
- Best estimate SCC growth rate of 0.80 mils/day (2.4×10^{-10} m/s)
- SCC initiated in less than 16 days

FIGURE 14

Characteristics of Weld Metal Used for Crack Growth Rate Specimens

Characteristic	
Filler Metal ID Carbon Level	EN82 761668S 0.009 w/o
Welding Process	Hot Wire Gas Tungsten
Welding Parameters Shielding gas Current Volts	 Argon 300 amps 12.5 v

0.4T Compact Tension Specimens were oriented such that the notch is perpendicular to the welding passes.

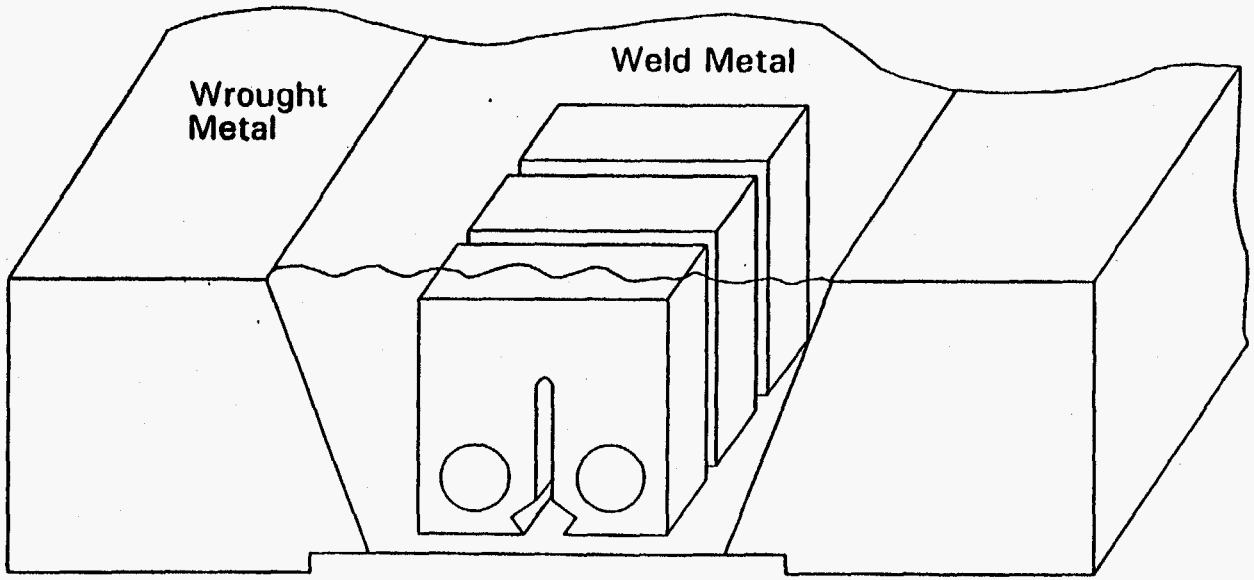

FIGURE 15

COMPARISON OF SCCGRs FOR EN82 WELD METAL SPECIMENS

Specimen I.D.	Test Time (days)	Crack Detection Time (days)	Cracking Time (days)	Maximum Crack Depth (mils)	SCCGR[1] (mils/day)	SCCGR [2] (mils/day)
7741 Side 1	108	3.60	104.40	112.3	1.08	0.95
7741 Side 2	108	3.60	104.40	95.9	0.92	0.83
0726 Side 1	108	3.40	104.60	67.8	0.65	0.56
0726 Side 2	108	3.40	104.60	79.8	0.76	0.69
7742 Side 1	108	15.90	92.10	67.8	0.74	0.74
7742 Side 2	108	15.90	92.10	56.8	0.62	0.62
				Overall Average	$\Sigma = 0.80$	$\Sigma = 0.74$

Notes: (1) SCCGR = (Maximum Crack Depth - Crack Depth at Detection)/Cracking Time
For this calculation, the crack depth at detection was assumed to be zero.

(2) SCCGR = (Maximum Crack Depth - Crack Depth at Detection)/Cracking Time
For this calculation, the crack depth at detection for specimens 7741 and 0726 were determined by correlating the total SCC area to the LVDT compliance. Due to a broken LVDT wire, a crack depth at detection could not be calculated for 7742 and was assumed to be zero.

FIGURE 16

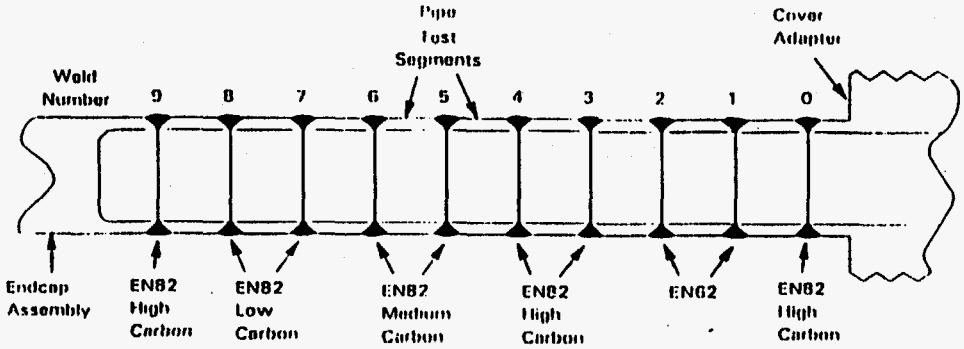

Cross sectional (schematic) view of test pipe assembly

Test Parameters

• Autoclave pressure	2850 psi (20 MPa)
• Water temperature	680°F (360°C)
• Hydrogen overpressure	40-60 cc/kg
• Axial load plus pressure	20.3 ksi (140 MPa)
• Axial tensile residual stress	30 ksi (207 MPa)
• Test duration	78 weeks

ALLOY 600 PIPE WELDMENT STRESS CORROSION TEST

- Axially loaded pipe specimen
- Nine 3" diameter Schedule 160 Alloy 600 pipe test segments
- Two heats of piping (good and bad microstructure)
- Total of 10 welds
  - 8 EN82 welds (2 low, 2 medium, 4 high carbon content)
  - 2 EN62 welds

FIGURE 17

SUMMARY OF POST-TEST EVALUATION OF PIPE WELDS

Weld No.	Met. Sect.	Penetrant Test Results	Ultrasonic Test Results	Weld Metal	Heat Affected Zone	Base Metal
1	A	1 circumferential linear indication, 1.0" long, root (U)	No indications	No cracks	2 cracks > 0.100" long, 0.015" deep (U) 0.013" deep (U)	No cracks
1	B	8 longitudinal linear indications: (5) 0.125" long, (3) 0.063" long, weld metal	No indications	1 longitudinal crack 0.020" long, 0.0075" deep	No cracks	No cracks
1	C	6 longitudinal linear indications: (4) 0.031" long, (2) 0.125" long, weld metal	No indications	No cracks	No cracks	No cracks
1	D	1 circumferential linear indication, 1.0" long; 3 longitudinal linear indications, 0.125" long, weld metal	No indications	No cracks	1 crack - < 0.001" deep (U)	No cracks
2	A	Lack of fusion, 0.700" long (A), scattered porosity	No indications	No cracks	1 crack - > 0.080" long, 0.024" deep (U)	No cracks
2	B	Scattered porosity	No indications	2 cracks > 0.060" long, 0.004" deep > 0.050" long, 0.008" deep	1 crack - 0.020" long, 0.005" deep (U)	No cracks
2	C	Scattered porosity	No indications	1 crack - 0.030" long, 0.009" deep	2 cracks > 0.030" long, 0.002" deep (U) > 0.010" long, 0.001" deep (U)	No cracks
2	E	Scattered porosity	1 indication weld metal	No cracks	No cracks	No cracks
3	B	Scattered porosity	No indications	No cracks	No cracks	No cracks
3	C	Scattered porosity	No indications	No cracks	No cracks	1 crack - 0.002" deep (A)
3	D	Scattered porosity	No indications	No cracks	2 cracks 0.001" deep (A) 0.007" deep (U)	1 crack - 0.002" deep (A), counterbore
4	B	Scattered porosity	No indications	3 cracks > 0.020" long, 0.003" deep > 0.020" long, 0.002" deep 0.002" deep	2 cracks > 0.060" long, 0.001" deep (U) > 0.040" long, 0.001" deep (A)	1 crack - > 0.060" long, 0.016" deep (A), counterbore

FIGURE 18

SUMMARY OF POST-TEST EVALUATION OF PIPE WELDS (CONTINUED)

Weld No.	Met. Sect.	Penetrant Test Results	Ultrasonic Test Results	Weld Metal	Heat Affected Zone	Base Metal
4	D	Scattered porosity	1 indication weld metal	No cracks	2 cracks > 0.020" long, 0.001" deep (U) 0.001" deep (A)	No cracks
5	B	Scattered porosity	No indications	No cracks	1 crack - > 0.020" long, 0.003" deep (U)	No cracks
6	A	Scattered porosity	No indications	No cracks	1 crack - 0.001" deep (U)	1 crack - 0.001" deep (A)
6	C	Scattered porosity	1 indication HAZ	1 crack - 0.0006" deep (A)	1 crack - > 0.04" long, 0.006" deep (U)	No cracks
6	D	Scattered porosity	1 indication HAZ	No cracks	1 crack - > 0.060" long, 0.007" deep (U)	1 crack - > 0.080" long, 0.007" deep (A), counterbore
7	A	Lack of fusion, 4.1" long (A). Linear porosoty, 2.1" long	No indication	No cracks	1 crack - > 0.060" long, 0.009" deep (U)	No cracks
7	B	5 diagonal linear indications, 0.060"-0.120" long, weld metal	No indications	2 cracks 0.002" deep 0.002" deep	1 crack - > 0.060" long, 0.024" deep (U)	No cracks
7	C	1 diagonal linear indication, 0.125" long, weld metal. Linear porosity, 0.700" long	1 indication base metal	1 crack - 0.001" deep	2 cracks > 0.060" long, 0.012" deep (U) > 0.060" long, 0.007" deep (A)	No cracks
8	B	Scattered porosity	1 indication HAZ	2 cracks 0.003" deep 0.001" deep	2 cracks > 0.080" long, 0.012" deep (U) > 0.080" long, 0.006" deep (A)	1 crack - > 0.080" long, 0.011" deep (U), counterbore
9	A	No indications	No indications	No cracks	1 crack - 0.020" long, 0.001" deep (A)	No cracks
0	B	No indications	No indications	No cracks	No cracks	No cracks

NOTES: Crack length was established by grinding and polishing incrementally until the crack disappeared.
If no crack length is shown, the crack had disappeared after the first increment (usually 0.020") was removed.
All cracks are circumferential unless otherwise indicated.

(A) Side of weld with acceptable microstructure base metal - NX8908
(U) Side of weld with unacceptable microstructure base metal - NX8913

Pipe wall thickness = 0.437" nominal

FIGURE 18A

Results

- SCC initiation observed in weld metal and HAZ of each weld

Location	Maximum Crack Depth (mils/mm)
Weld Metal	8.8/.22
HAZ	23.8/.60
Base Metal	16.0/.41

- EN62 and low carbon EN82 had highest propensity for weld SCC
- Worst HAZ SCC occurred in base metal with bad microstructure
- HAZ and base metal cracks initiated from stress concentrators

Alloy 600 Pipe Weldment Stress Corrosion Test
Longitudinal Section of Pipe Weld

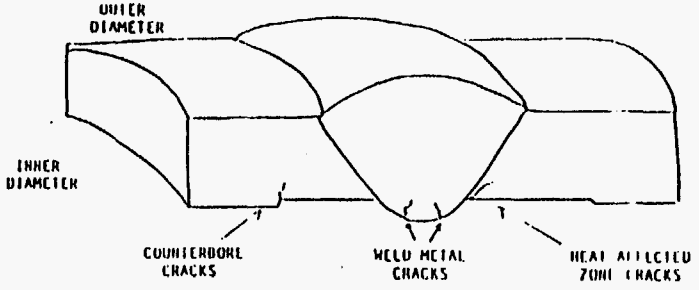

FIGURE 19

WELDING SEQUENCE

	Quadrant of Each Bead			
	Bead 1	Bead 2	Bead 3	Bead 4
Pass 1	IV	III	I	II
Pass 2	IV	II	III	I
Pass 3	III	I	II	IV
Pass 4	I	III	IV	II
Pass 5	III	I	IV	II
Pass 6	I	III	II	IV
Pass 7	III	I	II	IV

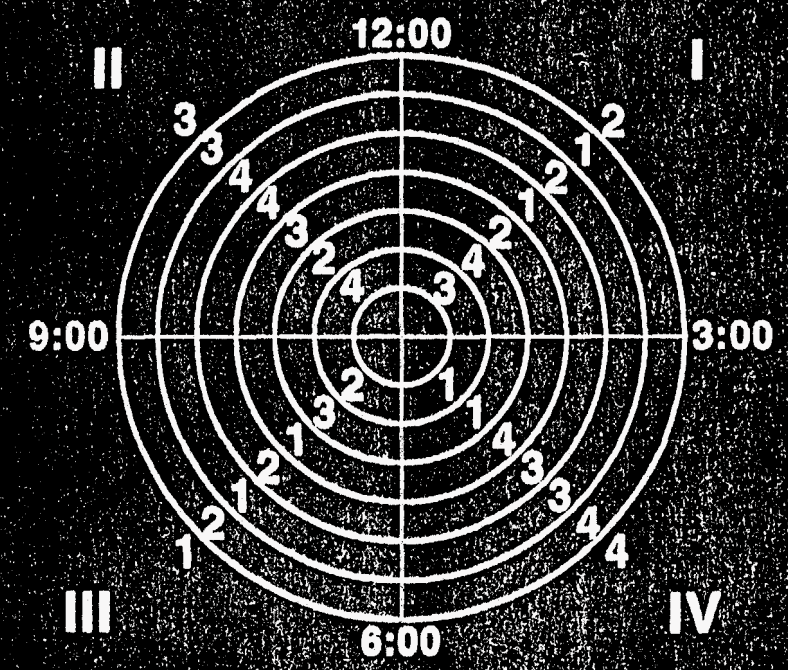

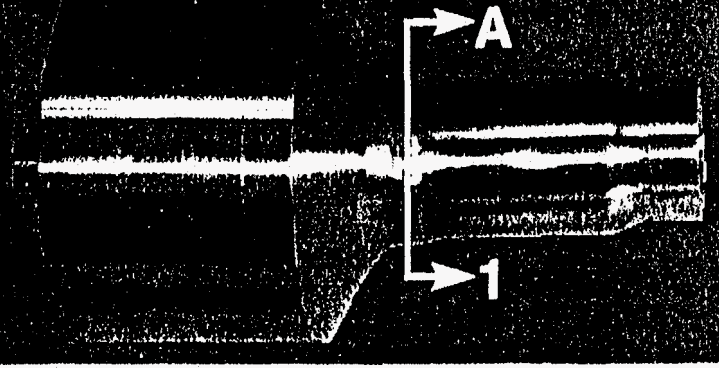

Knolls Atomic Power Laboratory

M7.cd

FIGURE 20

THERMAL BOUNDARY CONDITIONS

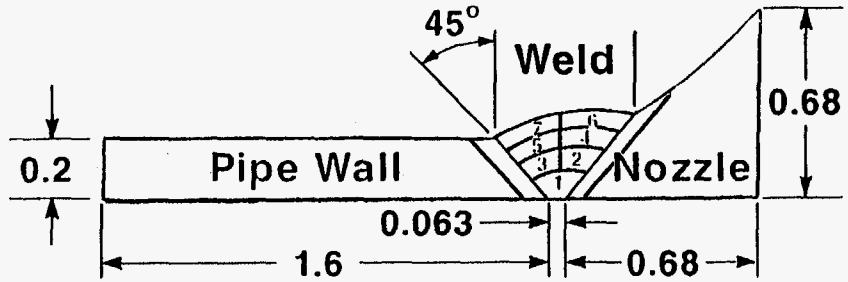

2.15" Weld Outer Dia
1.75" Weld Inner Dia

- Air with NC Heat Transfer
- Exterior Surface of Weld Elements Insulated After Birth
- Monitor Depth of Molten Zone (40-50 Mils Max)
- Thermal Constraint Equations for Uniform Weld Metal Cooling
- Internal Heat Generation in Weld Passes
- Timed Weld Element Heat Generation to Model Arc Travel Speed
- Adjusted Heat Generation Function to Match Thermocouple Data

Knolls Atomic Power Laboratory

FIGURE 21

STRUCTURAL MODEL & BOUNDARY CONDITIONS

- 5056 Nodes, 4227 Hex/8 Elements
- Fixed Supports at Base
- Planar But Not Parallel at Pipe End
- Elastic/Plastic Temperature Dependent Material Properties
- Bi-Linear Stress-Strain Curves [70°F to 2100°F]
- Kinematic Material Hardening
- Root Gap Set Using 3 Tack Welds
- Deposited 7 Full 360° Passes

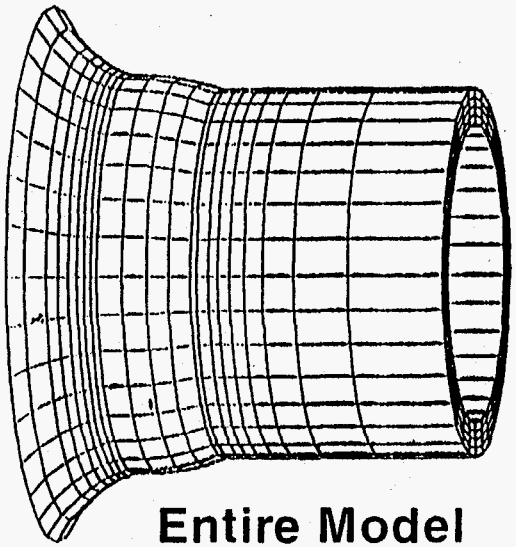

Entire Model

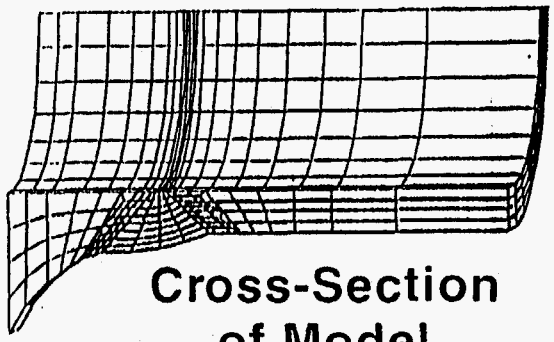

Cross-Section of Model

Knolls Atomic Power Laboratory

FIGURE 22

AXIAL STRESS SOLUTION

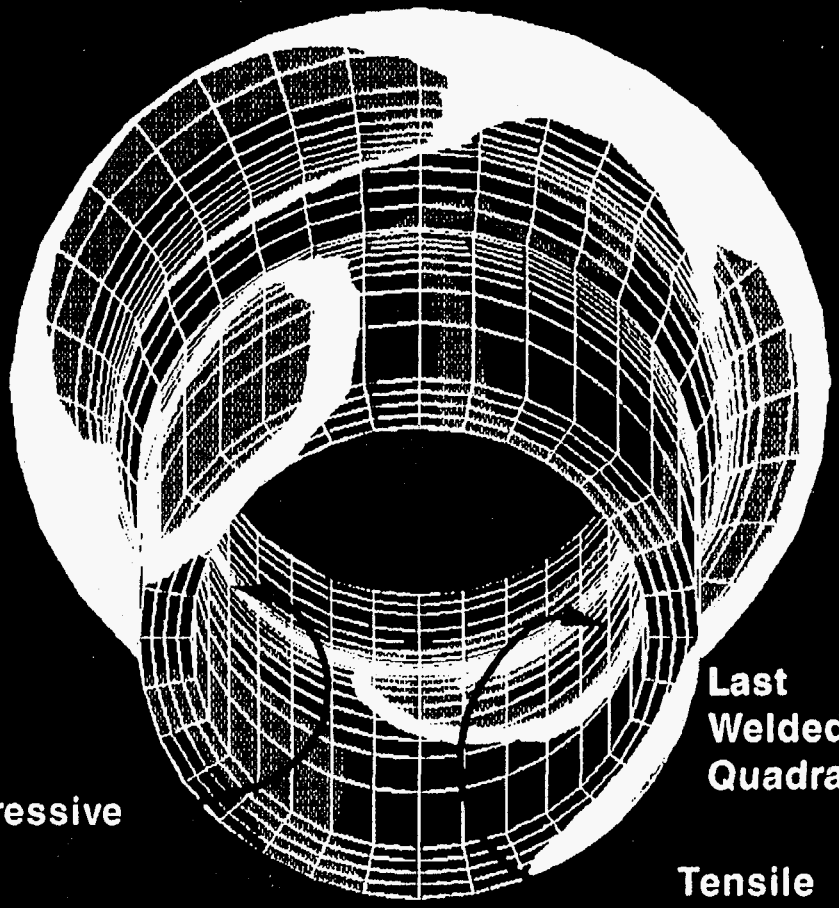

Knolls Atomic Power Laboratory

FIGURE 23

EXPERIMENTAL COMPARISONS

- Chemical Cracking Corroborated Peak Stress Locations
- Cracking at Locations Calculated Above 30-35 ksi

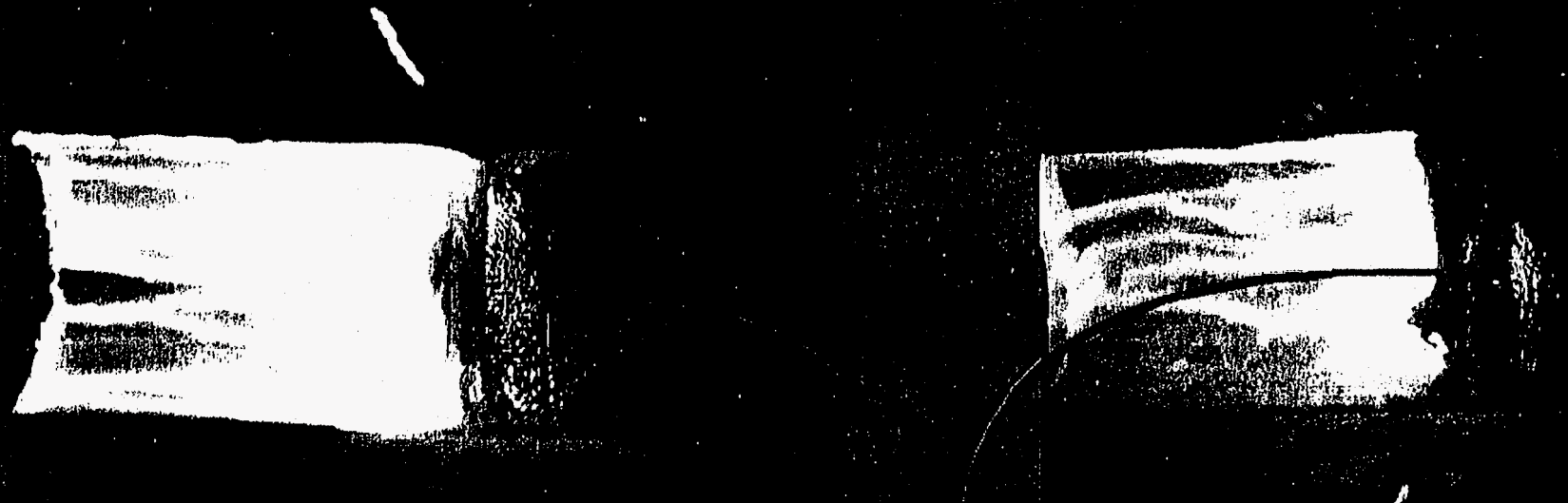

Last Welded Quadrant

180° Away

Zyglo of Cracking in Regions of
>30-35 ksi Tensile Axial Stress

Knolls Atomic Power Laboratory

M10.cd

FIGURE 24

EXPERIMENTAL COMPARISONS (CONTINUED)

Hole Drill 16 ID & OD Locations:
- **Matched ID Cyclic Stress Variation**
- **Calculated Stress Magnitudes Well**

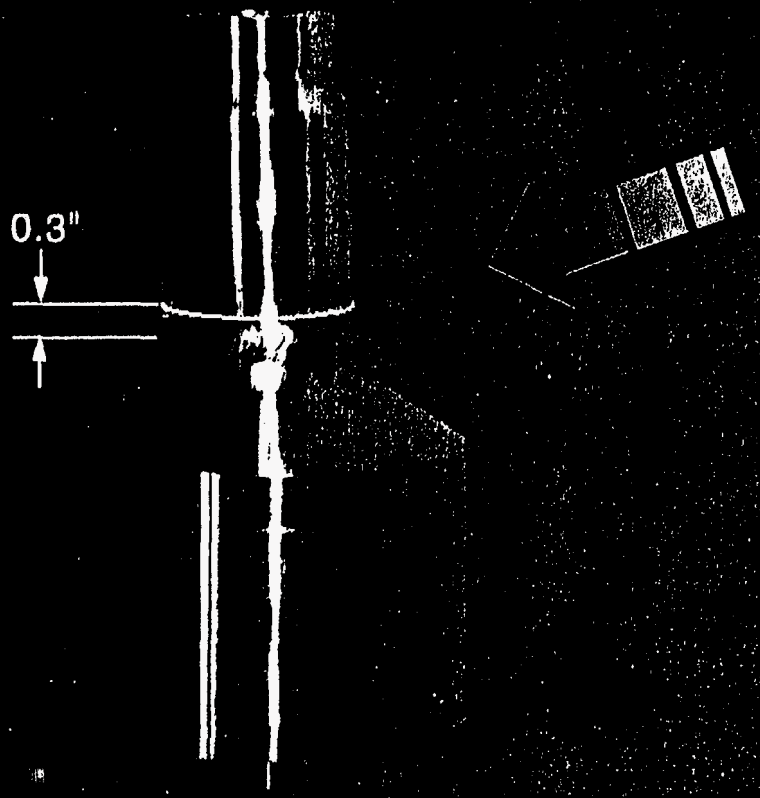

Hardware Mock-up

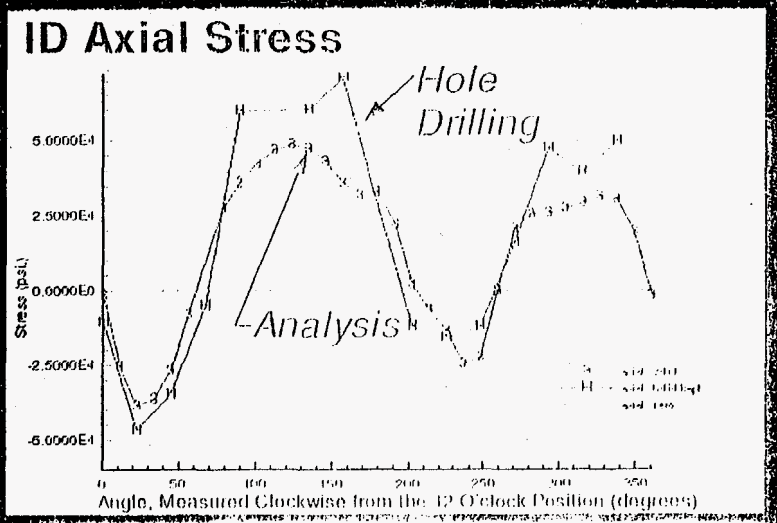

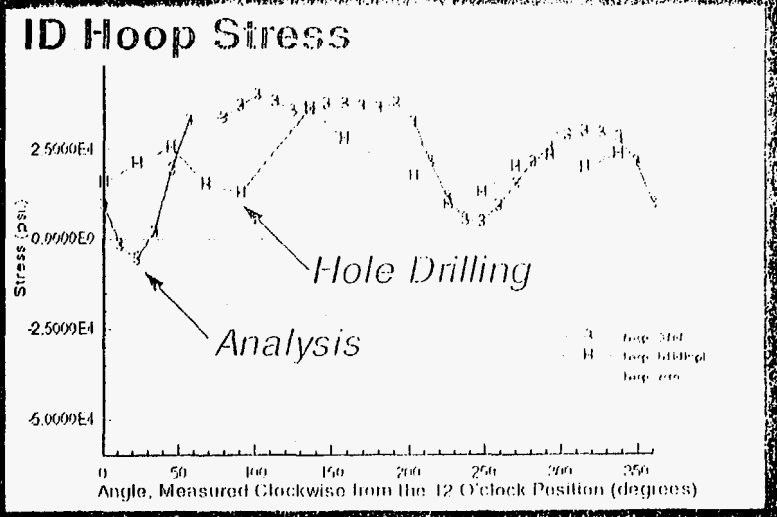

Knolls Atomic Power Laboratory

M11.cdr

FIGURE 25

COMPARE AXISYMMETRIC AND 3D SOLUTIONS

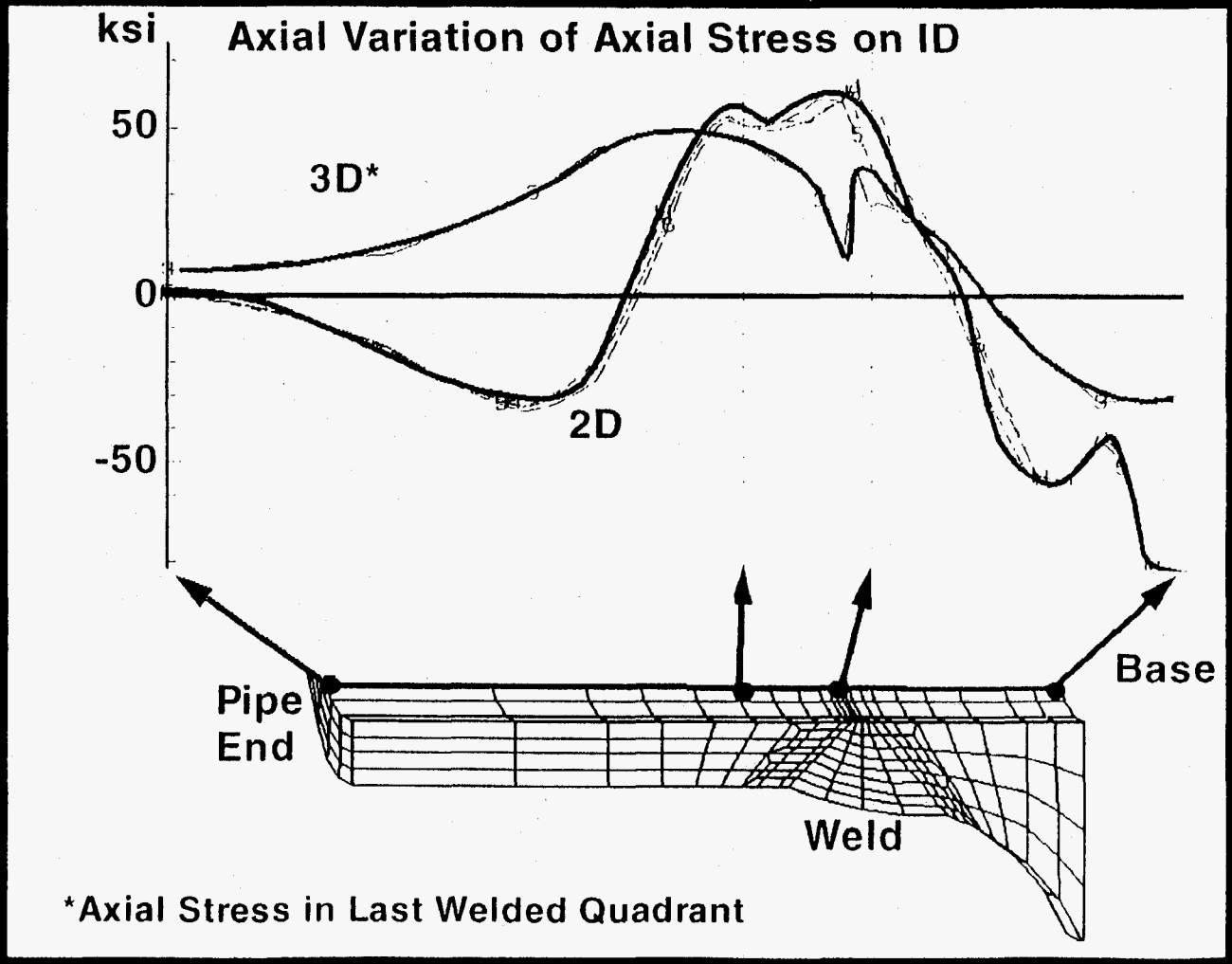

Knolls Atomic Power Laboratory

FIGURE 26

CONCLUSIONS

- Good First Order Effects of Welding Process
- 3D Analysis Necessary for True Weld-Induced Stress Response
- Expect Tensile Stresses in Last Welded Quadrant for Thin Wall Weld
- Axisymmetric Analysis Overpredicts Peak 3D Stresses Near Weld, Less Agreement Away from Weld
- Through Wall Bending Assumption Not Valid for Stress Measurement Techniques

FIGURE 27